NATIONAL ADVISORY COMMITTEE FOR AERONAUTICS

TECHNICAL NOTE 3092

HYDRODYNAMIC DRAG OF 12- AND 21-PERCENT-THICK SURFACE-PIERCING STRUTS

By Claude W. Coffee, Jr., and Robert E. McKann

Langley Aeronautical Laboratory
Langley Field, Va.

Washington
December 1953

Q

NATIONAL ADVISORY COMMITTEE FOR AERONAUTICS

TECHNICAL NOTE 3092

HYDRODYNAMIC DRAG OF 12- AND 21-PERCENT-THICK SURFACE-PIERCING STRUTS

By Claude W. Coffee, Jr., and Robert E. McKann

SUMMARY

The hydrodynamic drag of three surface-piercing untapered struts at approximately 0° angle of yaw was determined at depths up to 6 chords for speeds up to 80 fps at various angles of rake. Two struts had NACA 66_1-012 airfoil sections, one with a 4-inch chord and the other with an 8-inch chord. The third strut had an NACA 66_4-021 airfoil section and a 4-inch chord.

The section drag coefficient was determined from plots of drag against depth. Over the small range of Reynolds number where wind-tunnel data were available for comparison, the tank data, at subcavitation speeds, were in good agreement with wind-tunnel results. Raking the struts changed the section drag coefficient as expected because of the change in effective thickness ratio that resulted from raking. The drag coefficient due to the drag at the surface intersection was approximately constant at Froude numbers above 8.0 and at subcavitation speeds. Within the speed range investigated, no surface ventilation was observed for any of the struts. The inception of cavitation was noted at a speed higher than that predicted from two-dimensional-flow theory. This difference was probably due to the influence of the free-water surface on the pressure distribution.

INTRODUCTION

The present trend toward the use of underwater lifting surfaces on water-based aircraft and surface vessels has emphasized the need for drag data on supporting struts which pierce the water surface. Such data are limited; in addition, these data were generally obtained as tares during tests of lifting surfaces and the accuracy of the measurements for the strut alone is of dubious value because of the lack of sensitivity of the measuring instruments.

The present investigation conducted in the Langley tank no. 1 was made to determine the hydrodynamic drag of struts which pierce the water surface and the effect of thickness ratio, size, and angle of rake on the

drag. The speed range investigated is believed to be in the order of the actual speed range that would be encountered in practical applications.

SYMBOLS

c	strut chord parallel to undisturbed water surface, ft
d	depth of submersion of strut tip below undisturbed water surface, ft
t	strut thickness, ft
D_0	extrapolated drag for zero depth, lb
D_s	section drag, lb
D_t	tip drag, lb
D_T	total strut drag, lb
c_d	section drag coefficient, $\frac{D_s}{\frac{1}{2}\rho V^2 cd}$
V	speed, fps
V_C	speed of inception of cavitation, fps
F	Froude number, $V/\sqrt{gc}$
R	Reynolds number, Vc/ν
g	acceleration due to gravity, 32.2 ft/sec^2
ρ	mass density of water, varied from 1.966 to 1.969 slugs/cu ft
ν	kinematic viscosity of water, varied from 1.311×10^{-5} to 1.654×10^{-5} sq ft/sec

DESCRIPTION OF MODELS

The NACA 66-series airfoil sections were chosen for the strut models because of their high theoretical cavitation speeds, low drag, and small

frontal angles. A small frontal angle is desirable to reduce the water pileup at the intersection of the strut leading edge and the water surface.

Two struts had NACA 66_1-012 airfoil sections with chords of 4 and 8 inches in order to investigate the effect of scale. The third strut had an NACA 66_4-021 airfoil section and a 4-inch chord. The ordinates of the strut sections are given in table I and the cross sections of the three struts are shown in figure 1. All the struts had the submerged tip parallel to the undisturbed water surface. (See fig. 2.)

In the position with 30° angle of rake of the 4-inch-chord struts, the chord parallel to the undisturbed water surface became 4.62 inches. The thickness ratios decreased from 12 and 21 percent to 10.4 and 18.2 percent, respectively.

The struts were made of stainless steel with a yield strength of approximately 115,000 lb/sq in. and were polished to a smooth finish that gave a measured surface roughness of 8 to 10 rms microinches.

APPARATUS AND PROCEDURE

A description of the Langley tank no. 1 and towing carriage is given in reference 1. The single-component balance, supported from the main structural members of the towing carriage, is shown in figure 3. Basically, the balance consisted of a heavy floating frame supported by strain-gage beams from a rigid frame attached to the carriage. Interchangeable jaws which conformed to the contours of the individual struts were used in a clamping unit in the vertical plane. Adjustments necessary to maintain negligible angle of yaw were made by rotating the clamping unit in the horizontal plane. Wind-tunnel results indicated that small angles of yaw near 0° would have negligible effect on the drag; however, because of the interaction of side force with drag on the strain-gage balance, a side-force gage was used to set the angle of yaw to give a minimum side force. Corrections were made to the drag readings for the interactions resulting from the remaining small side forces.

A shield was provided to prevent wetting of the gear and strain gages. (See fig. 2.)

The drag was measured during constant-speed tests over a range of speed from 30 to 80 fps with the struts at 0° angle of yaw and depths of submersion ranging from 4 to 24 inches. The three struts were tested at 0° angle of rake and both 4-inch-chord struts were tested at ±30° angle of rake. The angle of rake was considered to be positive when the submerged tip was raked forward and negative when the submerged tip was raked aft (fig. 2). The output from the strain gages was read from a

microammeter or recorded by a pen-type strip recorder. The plotted drag data include the air drag of the length of strut exposed below the spray shield.

Spray photographs and underwater photographs were taken of the struts by using fixed-position flash equipment similar to that described in reference 2.

The accuracy of the basic measurements is believed to be within the following limits:

Drag, lb	±0.5
Speed, fps	±0.1

RESULTS AND DISCUSSION

Drag

The measured drag of the struts at the various angles of rake is plotted against speed in figure 4 with depth as a parameter. No data were obtained for the 12-percent-thick strut with 4-inch chord raked forward 30° because the strut became directionally unstable and failed in bending. The drag appeared to vary approximately as the square of the speed until cavitation occurred. The speed at which cavitation was first noticed is indicated by small vertical arrows. The drag increased rapidly as speed increased after the inception of cavitation.

The variation of drag with depth was obtained from figure 4 and is plotted in figure 5 with speed as a parameter. The total drag for a given speed before the inception of cavitation appeared to vary directly as the depth after a sufficient depth had been reached so that the surface intersection and tip effects became constant. At small depths where interaction occurs between the surface and tip effects, this interaction at 0° angle of rake is noted to have a consistently favorable effect on the drag.

The section drag at any speed was assumed to be

$$D_S = D_T - D_0$$

where D_0 was determined by extrapolating the straight-line portion of the total-drag curves (fig. 5) to zero depth.

The section drag coefficient, based on a static-immersed projected area, is plotted against Reynolds number in figure 6. Included in figure 6

is the Schoenherr line (ref. 3) that represents average skin-friction coefficients for fully turbulent flow on smooth flat plates and the Blasius line (ref. 4) that represents laminar flow. In general, the section drag coefficients for the various struts lie in the transition region between the laminar- and turbulent-flow lines and decrease with increasing Reynolds number.

In general, raking the struts either forward or rearward reduced the section drag coefficient from that for 0° angle of rake as would be expected from the change in effective thickness ratio that resulted from raking. The section drag coefficients obtained for the two 12-percent-thick struts were in good agreement and no effect of scale was indicated in the range of Reynolds number investigated. Wind-tunnel data for these airfoil sections, at the range of Reynolds number of these tests, are meager; but the wind-tunnel results (ref. 5) that can be compared with the tank data are in good agreement (fig. 6). This agreement indicates that wind-tunnel data may be used to estimate section drag coefficients for surface-piercing untapered struts operating at subcavitation speeds at 0° angle of yaw.

Values for the drag of the strut tip D_t were estimated by using the drag coefficient for square tips given in reference 6. By subtracting the tip drag from the extrapolated drag at zero depth, a value for the drag at the surface intersection was obtained at subcavitation speeds and was expressed in coefficient form as

$$\frac{D_0 - D_t}{\frac{1}{2}\rho V^2 ct}$$

Figure 7 indicates that, for all the struts tested, this coefficient was approximately constant at Froude numbers above 8.0 and at subcavitation speeds. All data for which cavitation was known to exist were omitted from figure 7; however, the data point at a Froude number of 24.4, representing the coefficient for the 12-percent-thick strut with the 4-inch chord at 80 fps, was appreciably higher than data points for coefficients corresponding to lower speeds. At 80 fps this strut may have just started to cavitate, but the cavitation had not developed to such an extent that it was visible.

Spray

Photographs showing the typical effect of spray around the strut at different speeds and depths are presented in figure 8. From these photographs, the spray height at the trailing edge was determined and is plotted against speed in figure 9. As would be expected, the spray height is

independent of the depth of submergence over the range of depth investigated. An increase in speed from 30 to 80 fps increased the spray height at the strut trailing edge approximately 30 percent.

The effect of strut size and thickness ratio on spray can be seen from a comparison of the photographs presented in figure 10. For struts having the same airfoil section (figs. 10(a) and (b)) tested at the same speed, the spray height at the strut trailing edge appears to be in direct proportion to the size of the strut. For the struts having the same chord but different thickness ratios (figs. 10(b) and (c)), the spray height at the trailing edge was greater for the thicker strut.

Photographs showing the typical effect of angle of rake on the spray height at the trailing edge of the 21-percent-thick strut are presented in figure 11. The effect of angle of rake on the height of the spray at the strut trailing edge was to reduce progressively the spray height as the strut was raked from 30° to 0° to -30°. The spray height at the strut trailing edge was measured perpendicular to the water surface.

Photographs showing the typical effect of thickness ratio on the two 4-inch-chord struts raked -30° are shown in figure 12. As was noticed in figures 10(b) and (c), the thick strut again has the higher spray at the strut trailing edge.

Cavitation and Ventilation

The 12-percent-thick struts gave no visible evidence of cavitation in the speed range investigated. The computed cavitation speed for this strut is approximately 83 fps.

Underwater photographs showing effects of speed on cavitation on the 21-percent-thick strut at 0° angle of rake are presented in figure 13. Visual observation and the break in the drag curves (fig. 4) indicate that the inception of cavitation in these tests occurred at speeds greater than the theoretical cavitation speed of 59 fps which was based on the pressure distribution that would be obtained in two-dimensional flow. The greatest delay in the inception of cavitation was at the 4-inch depth where visible cavitation did not start until a speed of approximately 70 fps had been reached. Cavitation did not begin near the water surface as might be expected on the basis of static pressure since apparently the proximity of the water surface resulted in an alteration of the pressure distribution and reduction of the pressure peak with consequent increase in the speed required for cavitation. The inception of cavitation occurred approximately at the 60-percent-chord station, the design location of minimum pressure. Raking the strut forward or aft caused a small increase in the speed at which cavitation was first observed from that for the unraked strut (figs. 4(d), (e), and (f)).

No surface ventilation was observed for any of the struts over the range of speed and angle of rake investigated. The intersection of the strut with the water surface as seen in the underwater photographs of figure 13 was typical of all the struts tested.

CONCLUSIONS

An investigation made to determine the hydrodynamic drag of three surface-piercing untapered struts at approximately 0° angle of yaw at depths up to 6 chords for speeds up to 80 fps and at various angles of rake indicates the following conclusions:

1. The section drag coefficients at subcavitation speeds were in good agreement with wind-tunnel results over the small range of Reynolds number where wind-tunnel data were available for comparison.

2. Raking the struts reduced the section drag coefficient from that with an angle of rake of 0° as would be expected from the change in effective thickness ratio that resulted from raking.

3. The drag coefficient due to the drag at the surface intersection was approximately constant at Froude numbers above 8.0 and at subcavitation speeds.

4. The inception of cavitation was noted at a speed higher than that predicted from two-dimensional-flow theory, probably because of the influence of the free-water surface on the pressure distribution.

5. No surface ventilation was observed on any of the struts over the range of speed and angle of rake investigated.

Langley Aeronautical Laboratory,
National Advisory Committee for Aeronautics,
Langley Field, Va., October 8, 1953.

REFERENCES

1. Truscott, Starr: The Enlarged N.A.C.A. Tank, and Some of Its Work. NACA TM 918, 1939.

2. Kapryan, Walter J., and Weinstein, Irving: The Planing Characteristics of a Surface Having a Basic Angle of Dead Rise of 20° and Horizontal Chine Flare. NACA TN 2804, 1952.

3. Davidson, Kenneth S. M.: Resistance and Powering. Detailed Considerations – Skin Friction. Vol. II of Principles of Naval Architecture, ch. II, pt. 2, sec. 7, Henry E. Rossell and Lawrence B. Chapman, eds., Soc. Naval Arch. and Marine Eng., 1939, pp. 76-83.

4. Blasius, H.: The Boundary Layers in Fluids With Little Friction. NACA TM 1256, 1950.

5. Abbott, Ira H., Von Doenhoff, Albert E., and Stivers, Louis S., Jr.: Summary of Airfoil Data. NACA Rep. 824, 1945. (Supersedes NACA WR L-560.)

6. Hoerner, Sighard F.: Aerodynamic Drag. Publ. by the author (148 Busteed, Midland Park, N. J.), 1951.

TABLE I.- ORDINATES OF STRUT SECTIONS

[All dimensions are in inches]

NACA 66_1-012 airfoil section, 4-inch chord		NACA 66_1-012 airfoil section, 8-inch chord		NACA 66_4-021 airfoil section, 4-inch chord	
Station	Ordinate	Station	Ordinate	Station	Ordinate
0	0	0	0	0	0
.05	.054	.10	.109	.05	.090
.10	.072	.20	.145	.10	.122
.20	.100	.40	.200	.20	.171
.40	.140	.80	.280	.40	.242
.80	.192	1.60	.384	.80	.335
1.20	.223	2.40	.445	1.20	.390
1.40	.232	2.80	.464	1.40	.406
1.60	.238	3.20	.476	1.60	.416
1.80	.240	3.60	.480	1.80	.420
2.00	.239	4.00	.477	2.00	.417
2.20	.233	4.40	.467	2.20	.407
2.40	.224	4.80	.447	2.40	.388
2.80	.181	5.60	.361	2.80	.304
3.20	.118	6.40	.236	3.20	.192
3.60	.049	7.20	.099	3.60	.077
3.80	.019	7.60	.038	3.80	.029
4.00	0	8.00	0	4.00	0
L.E. radius: 0.038		L.E. radius: 0.076		L.E. radius: 0.102	

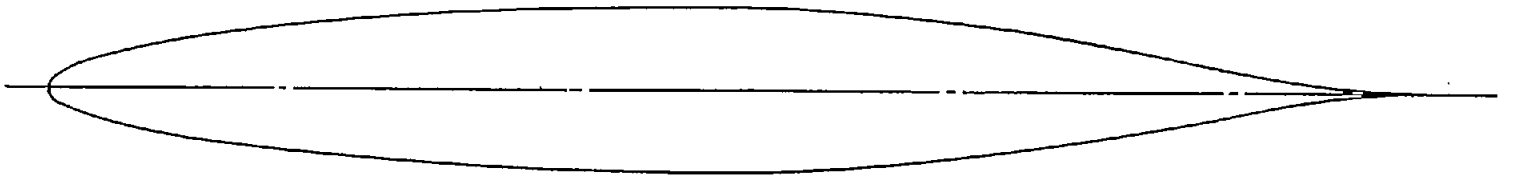

(a) NACA 66_1-012 airfoil section with 8-inch chord.

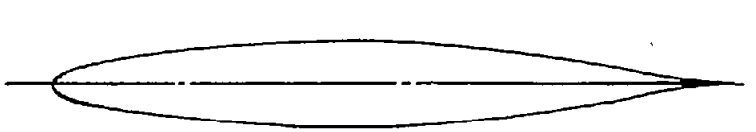

(b) NACA 66_1-012 airfoil section with 4-inch chord.

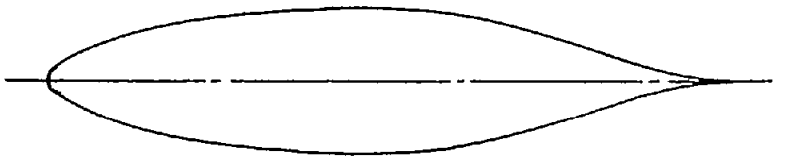

(c) NACA 66_4-021 airfoil section with 4-inch chord.

Figure 1.- Strut cross sections.

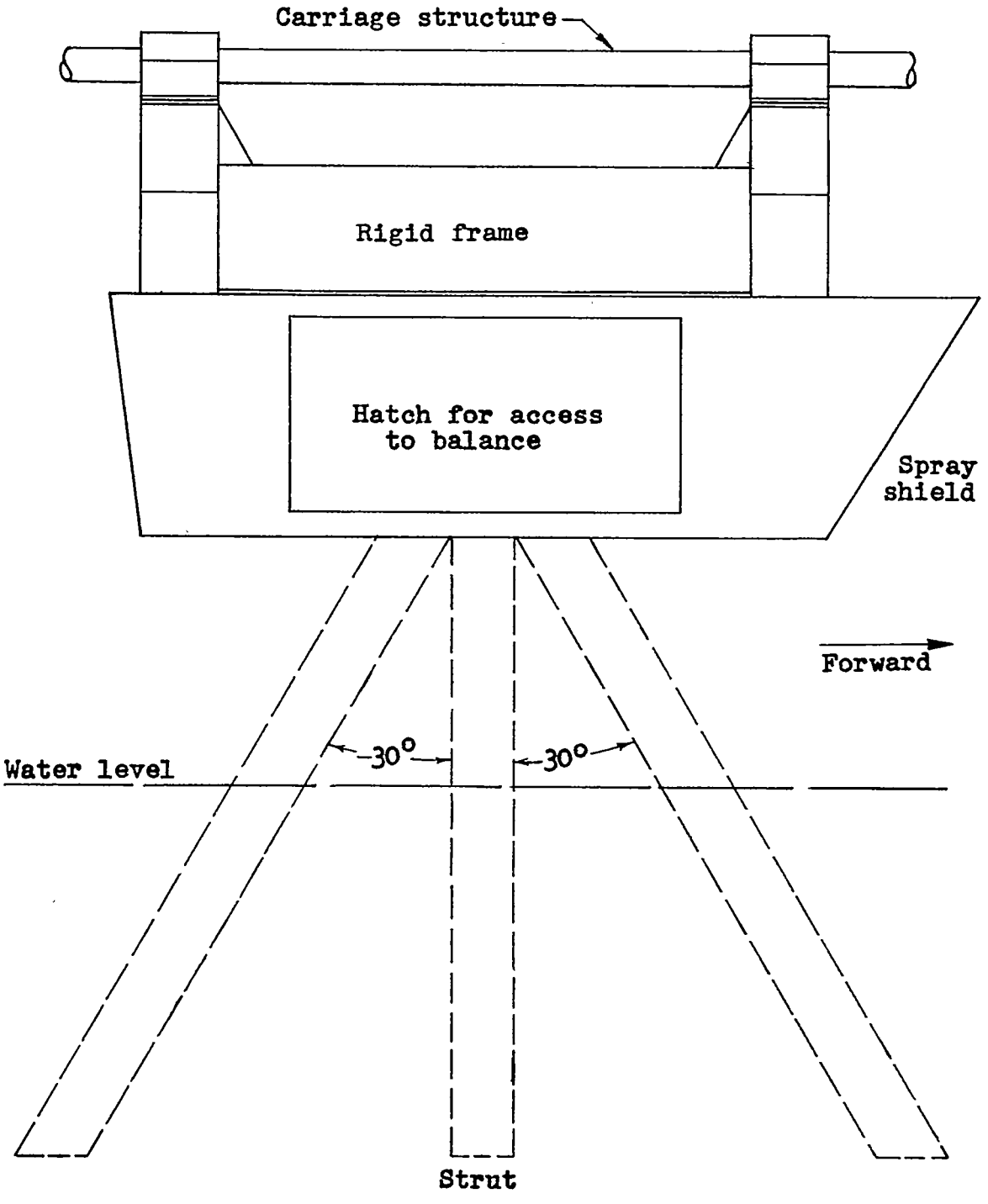

Figure 2.- Spray shield and typical strut at three angles of rake.

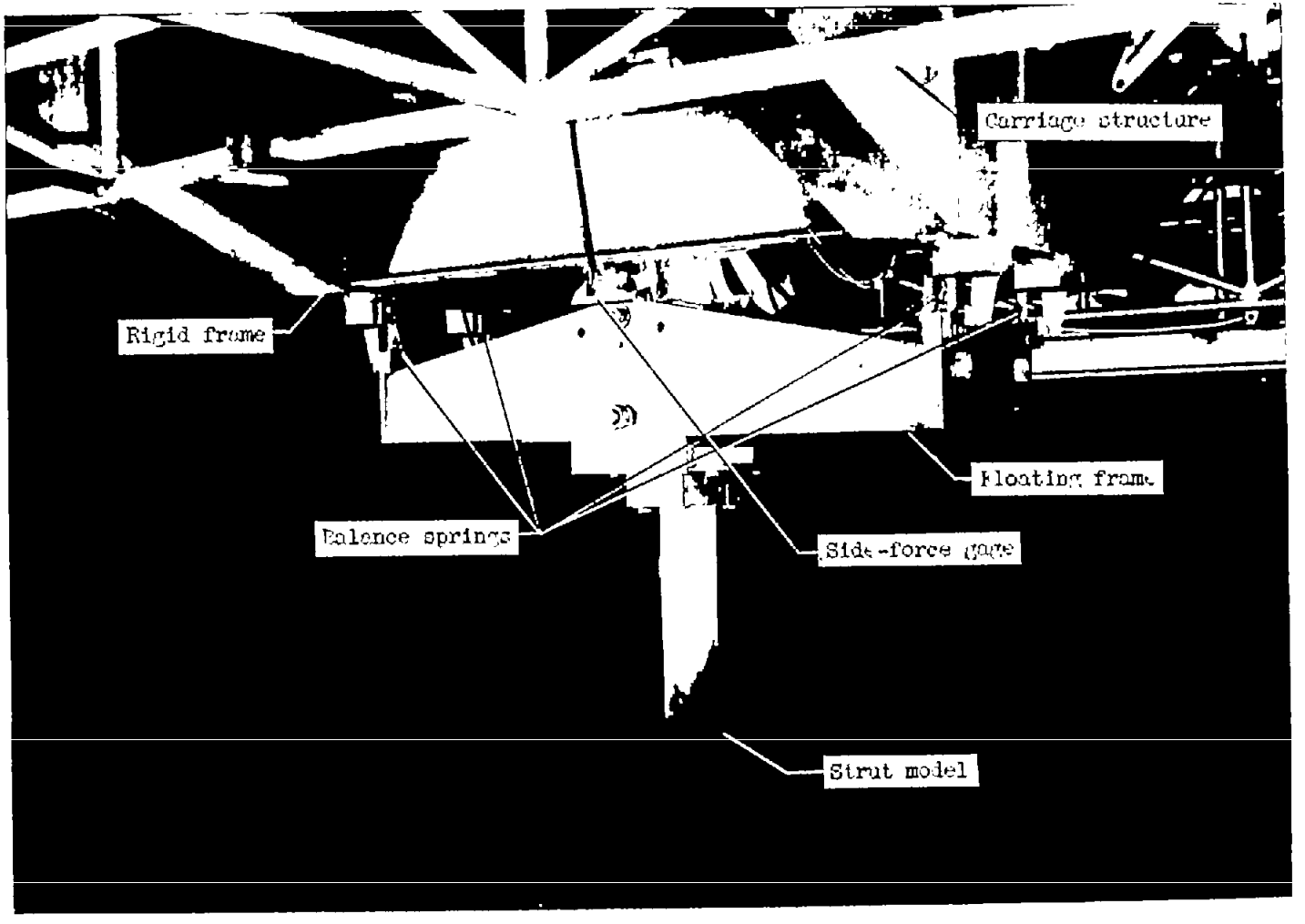

L-81265

Figure 3.- Test setup showing drag balance and strut attached to towing carriage.

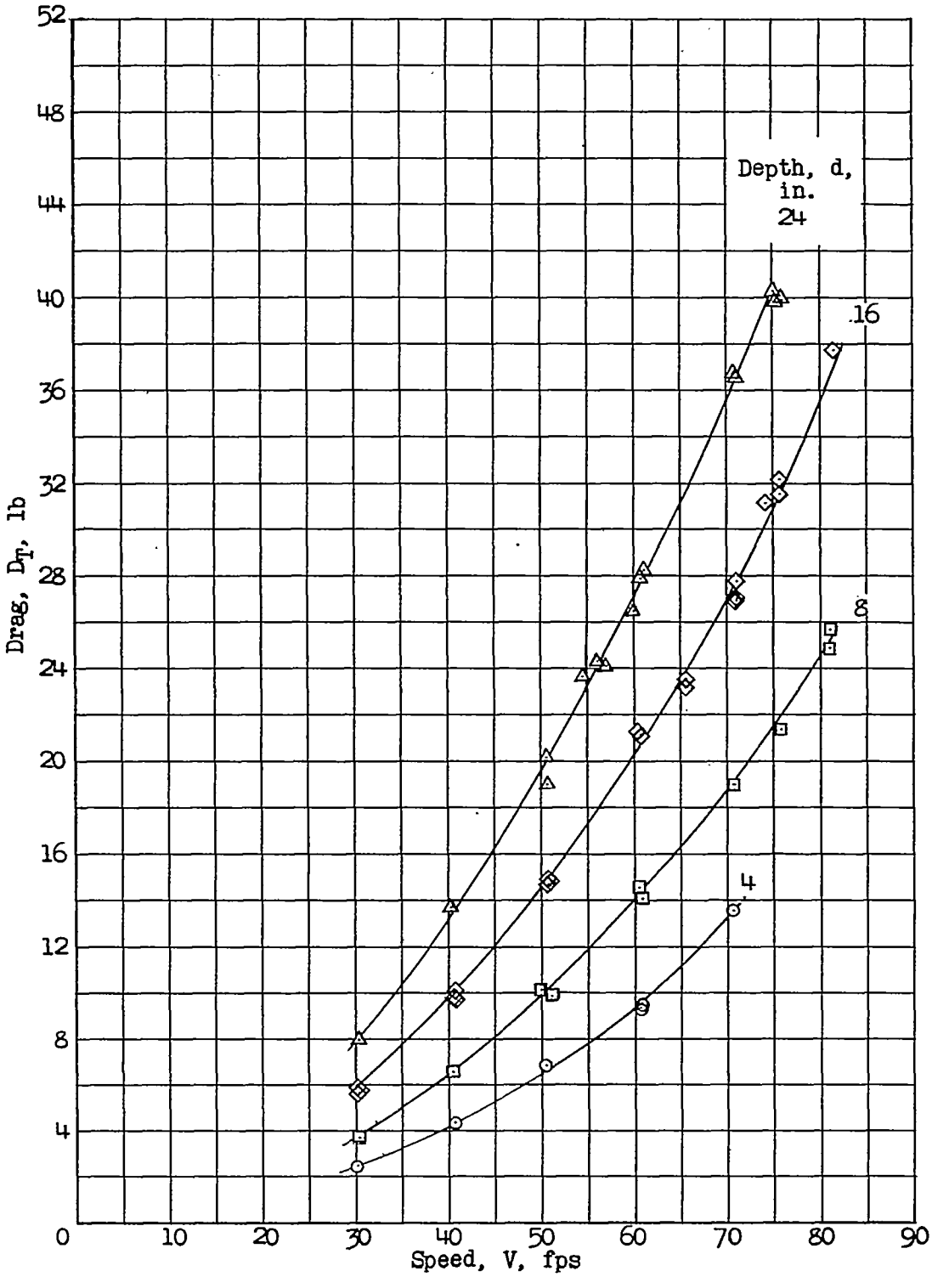

(a) NACA 66_1-012 airfoil section with 8-inch chord. Angle of rake, 0°.

Figure 4.- Variation of drag with speed.

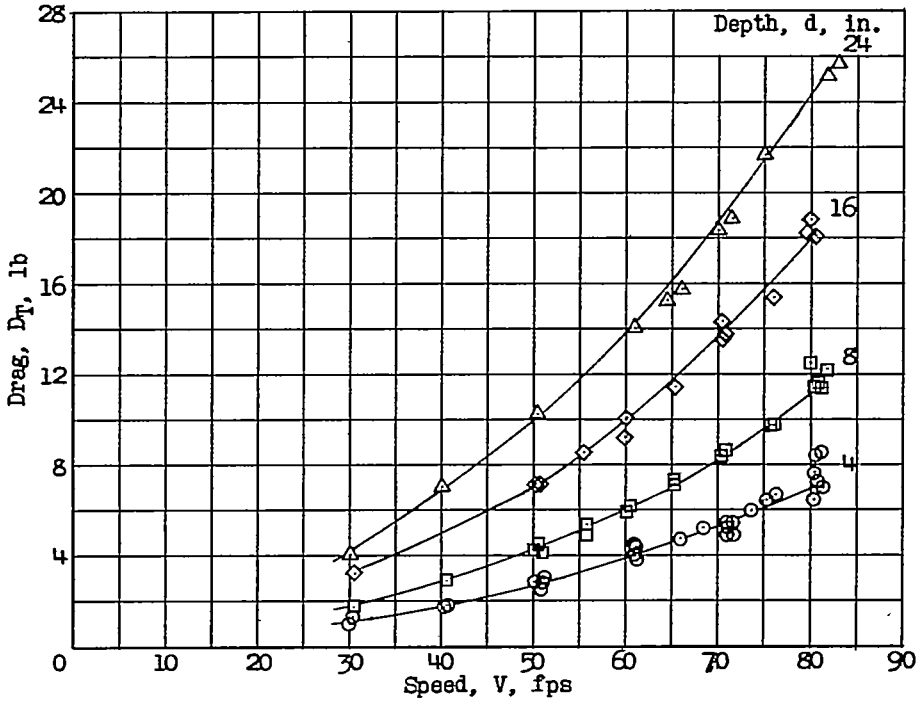

(b) NACA 66_1-012 airfoil section with 4-inch chord. Angle of rake, 0°.

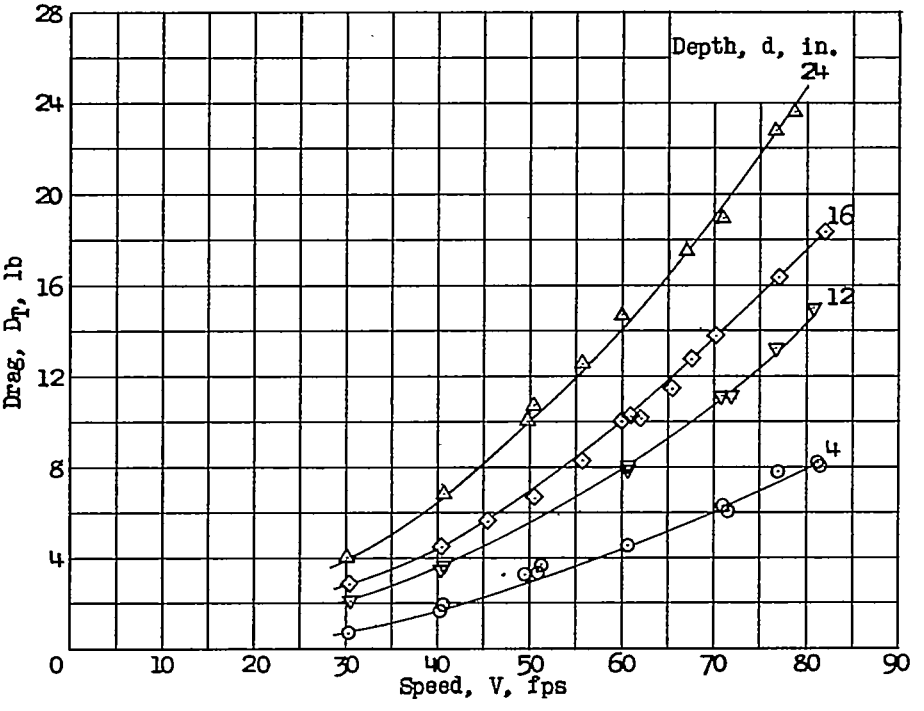

(c) NACA 66_1-012 airfoil section with 4-inch chord. Angle of rake, -30°.

Figure 4.- Continued.

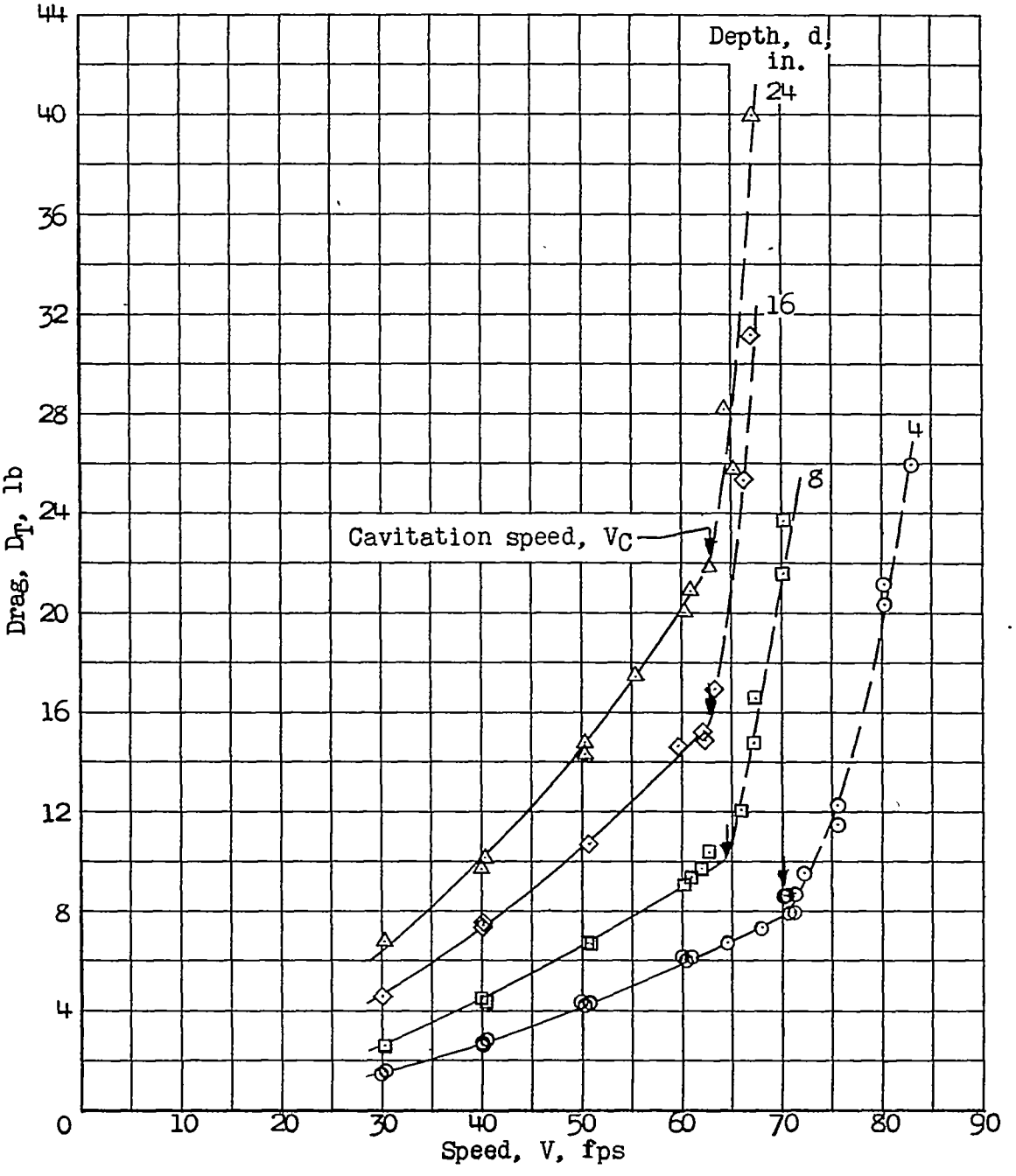

(d) NACA 66_4-021 airfoil section with 4-inch chord. Angle of rake, 0°.

Figure 4.- Continued.

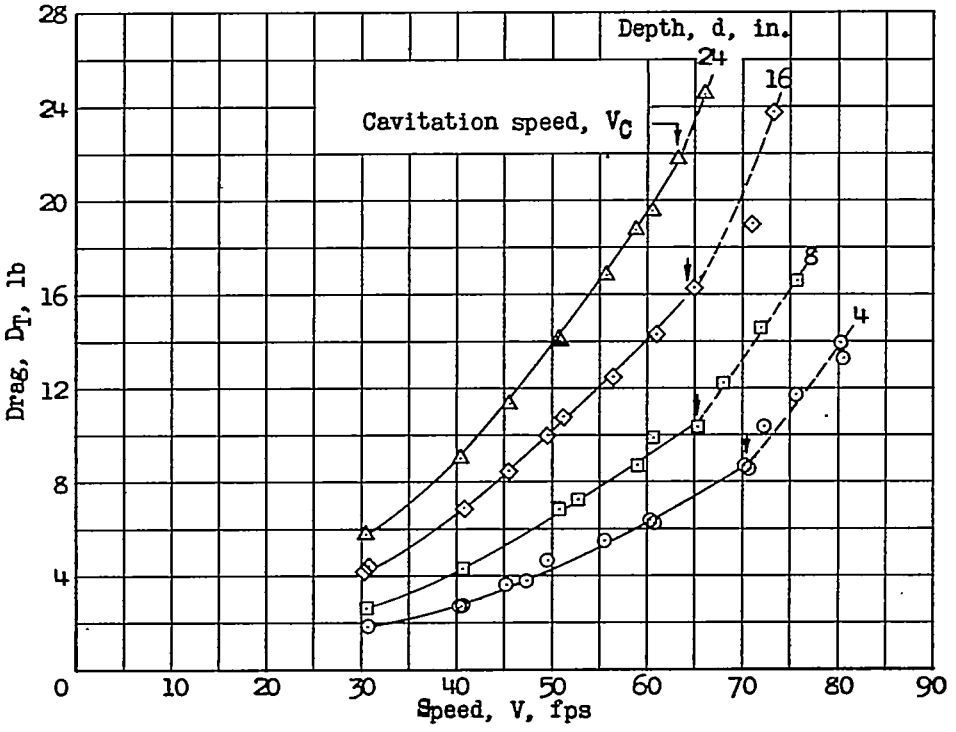

(e) NACA 66_4-021 airfoil section with 4-inch chord. Angle of rake, -30°.

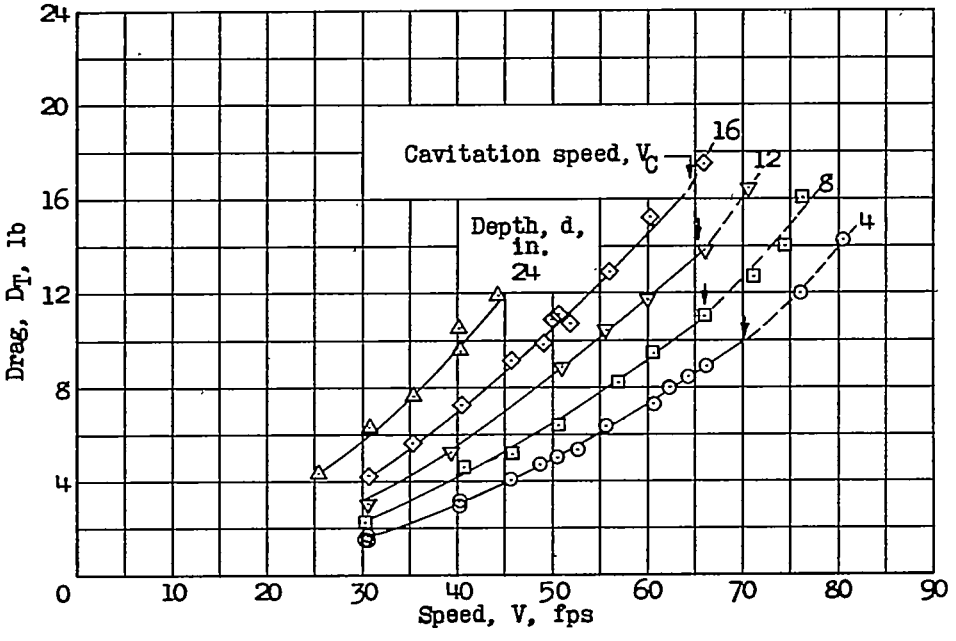

(f) NACA 66_4-021 airfoil section with 4-inch chord. Angle of rake, 30°.

Figure 4.- Concluded.

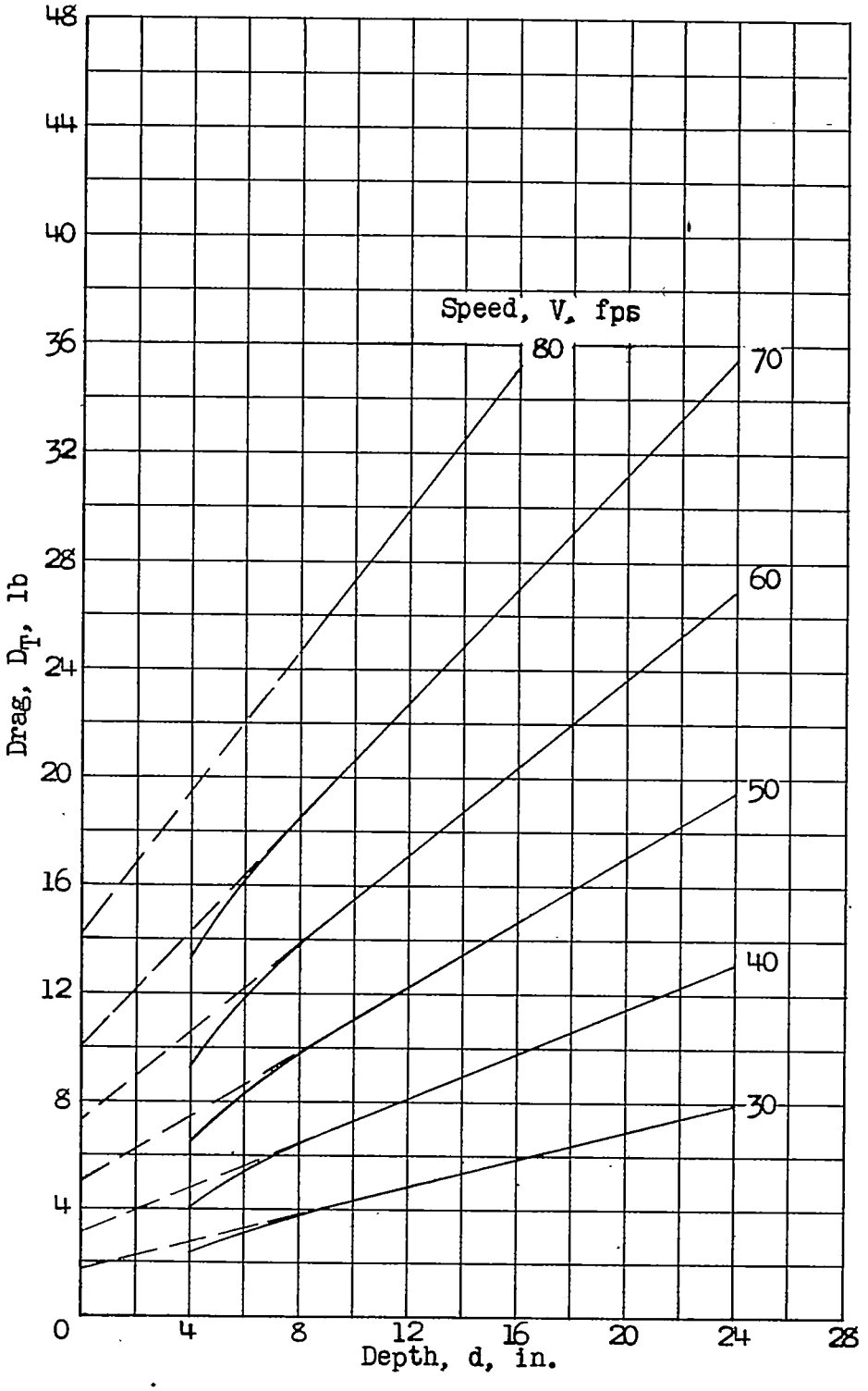

(a) NACA 66_1-012 airfoil section with 8-inch chord. Angle of rake, 0°.

Figure 5.- Variation of drag with depth.

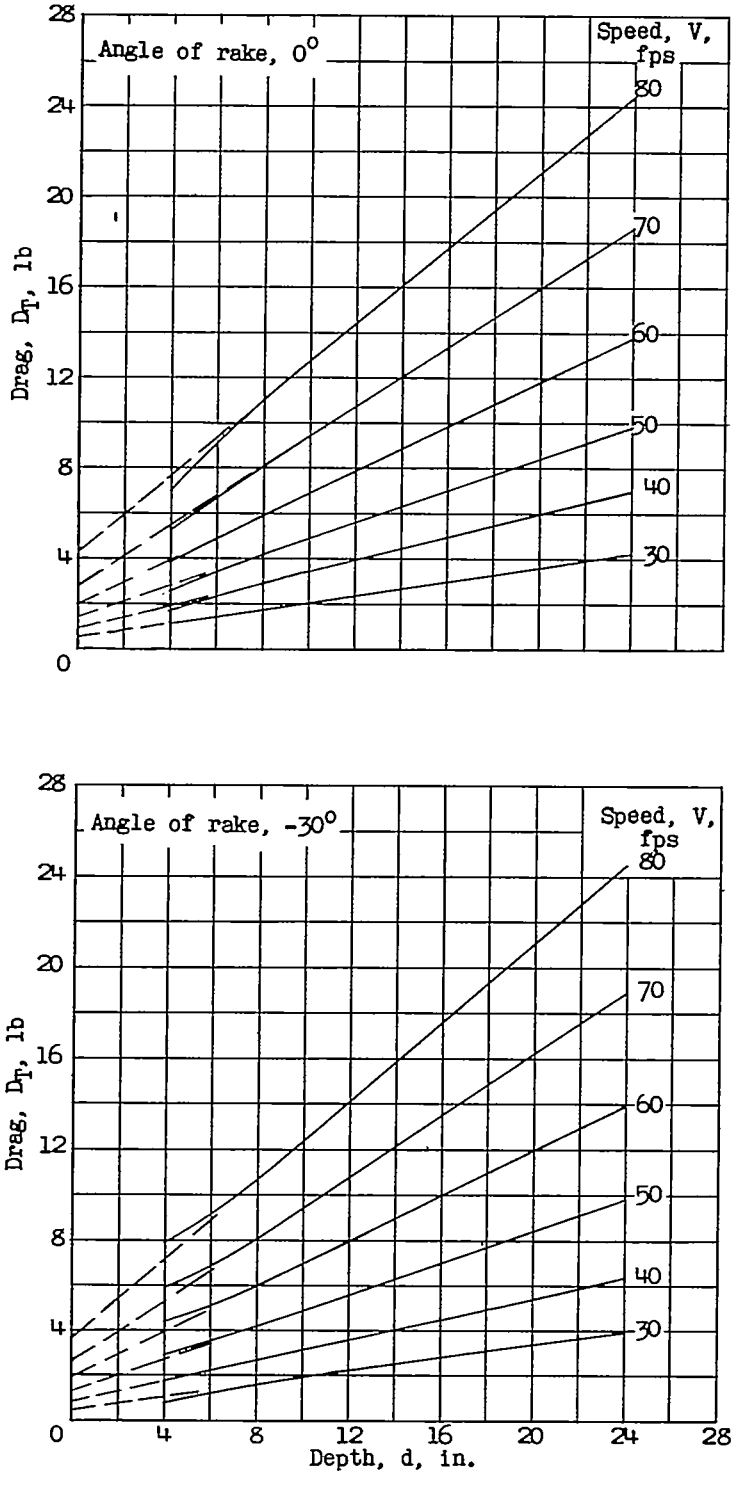

(b) NACA 66_1-012 airfoil section with 4-inch chord.

Figure 5.- Continued.

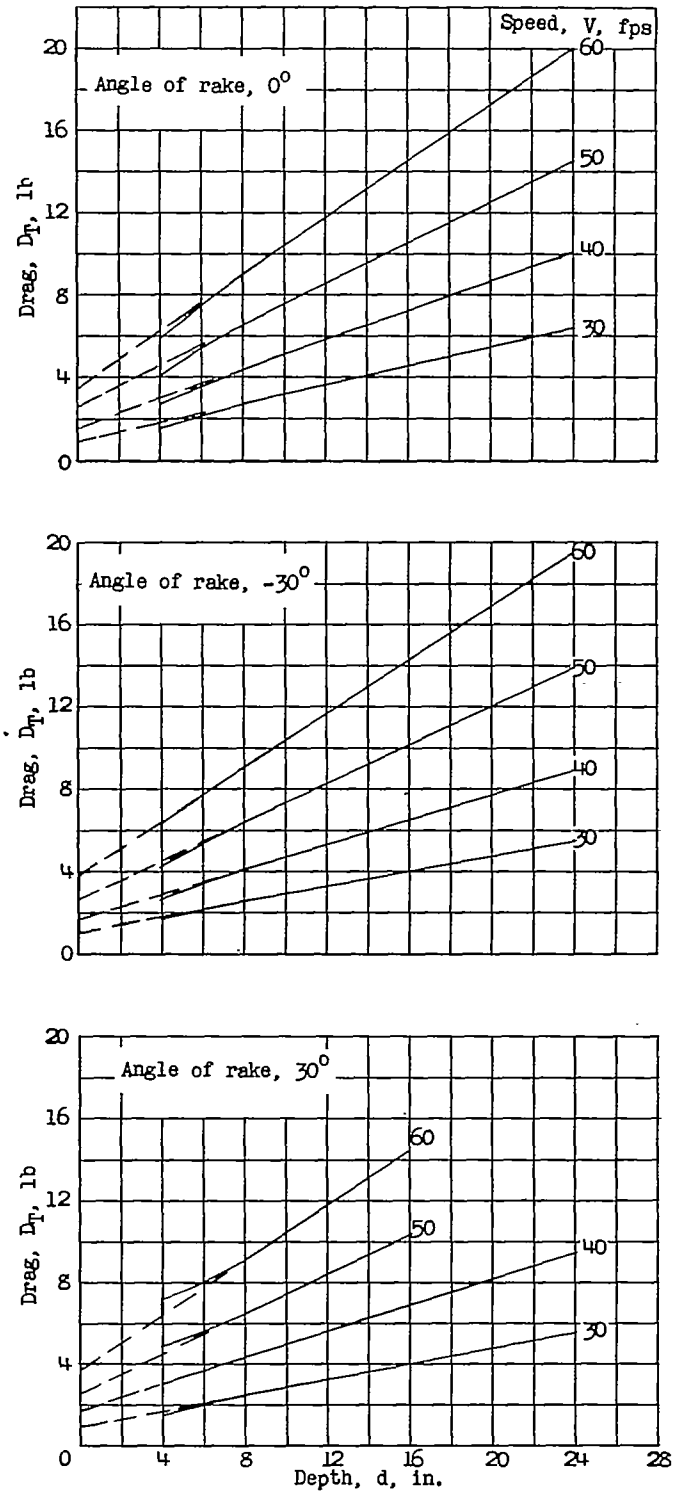

(c) NACA 66_4-021 airfoil section with 4-inch chord.

Figure 5.- Concluded.

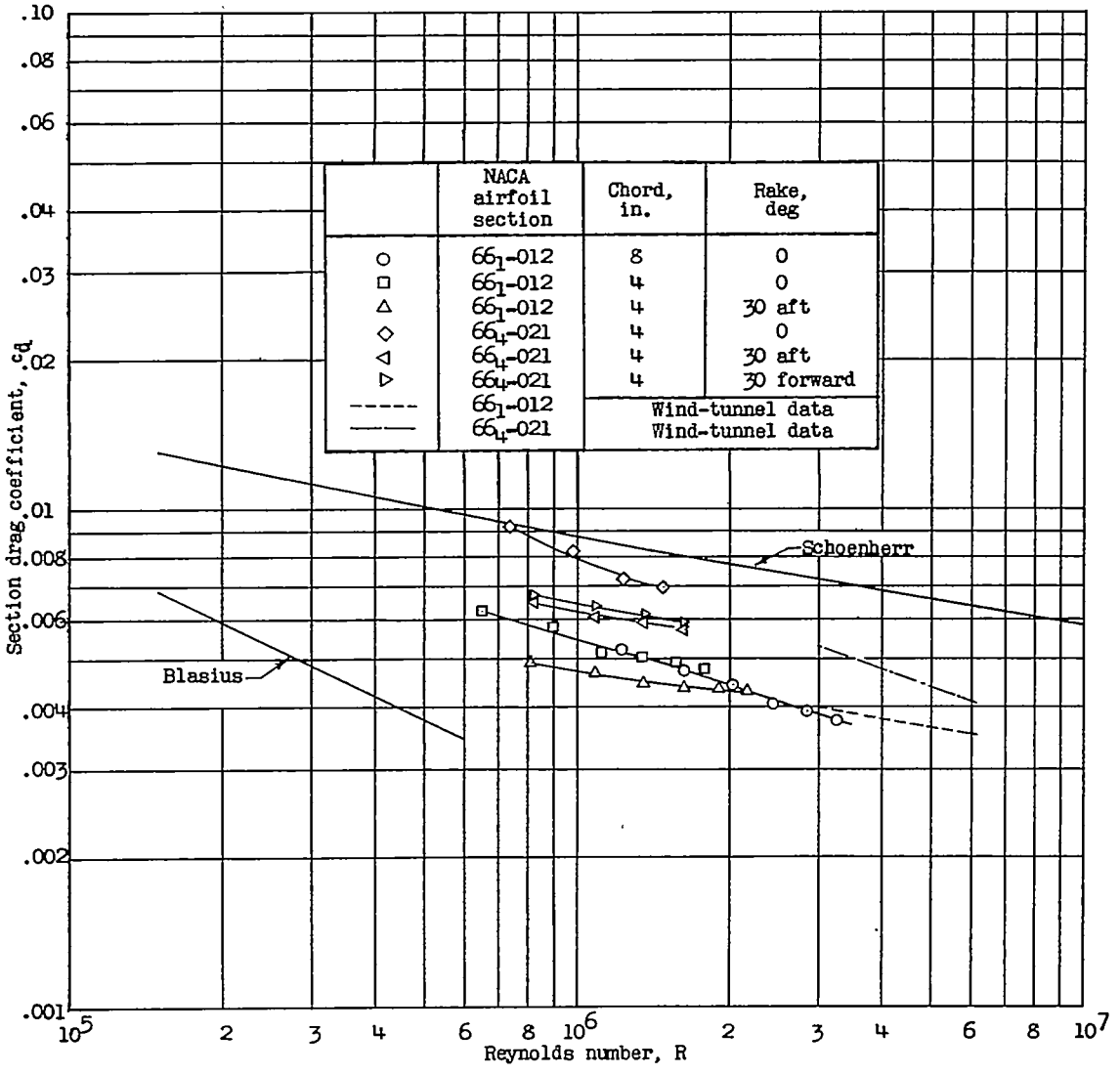

Figure 6.- Variation of section drag coefficient with Reynolds number.

	NACA airfoil section	Chord, in.	Rake, deg
○	66_1-012	8	0
□	66_1-012	4	0
△	66_1-012	4	30 aft
◇	66_4-021	4	0
◁	66_4-021	4	30 aft
▷	66_4-021	4	30 forward

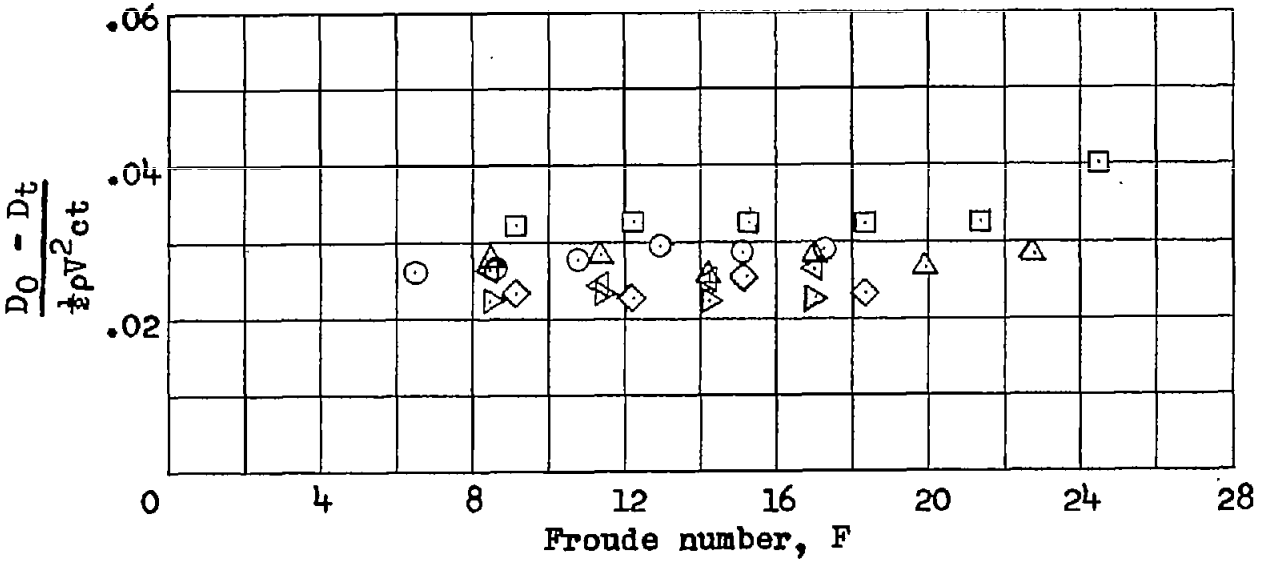

Figure 7.- Variation of $\frac{D_0 - D_t}{\frac{1}{2}\rho V^2 ct}$ with Froude number.

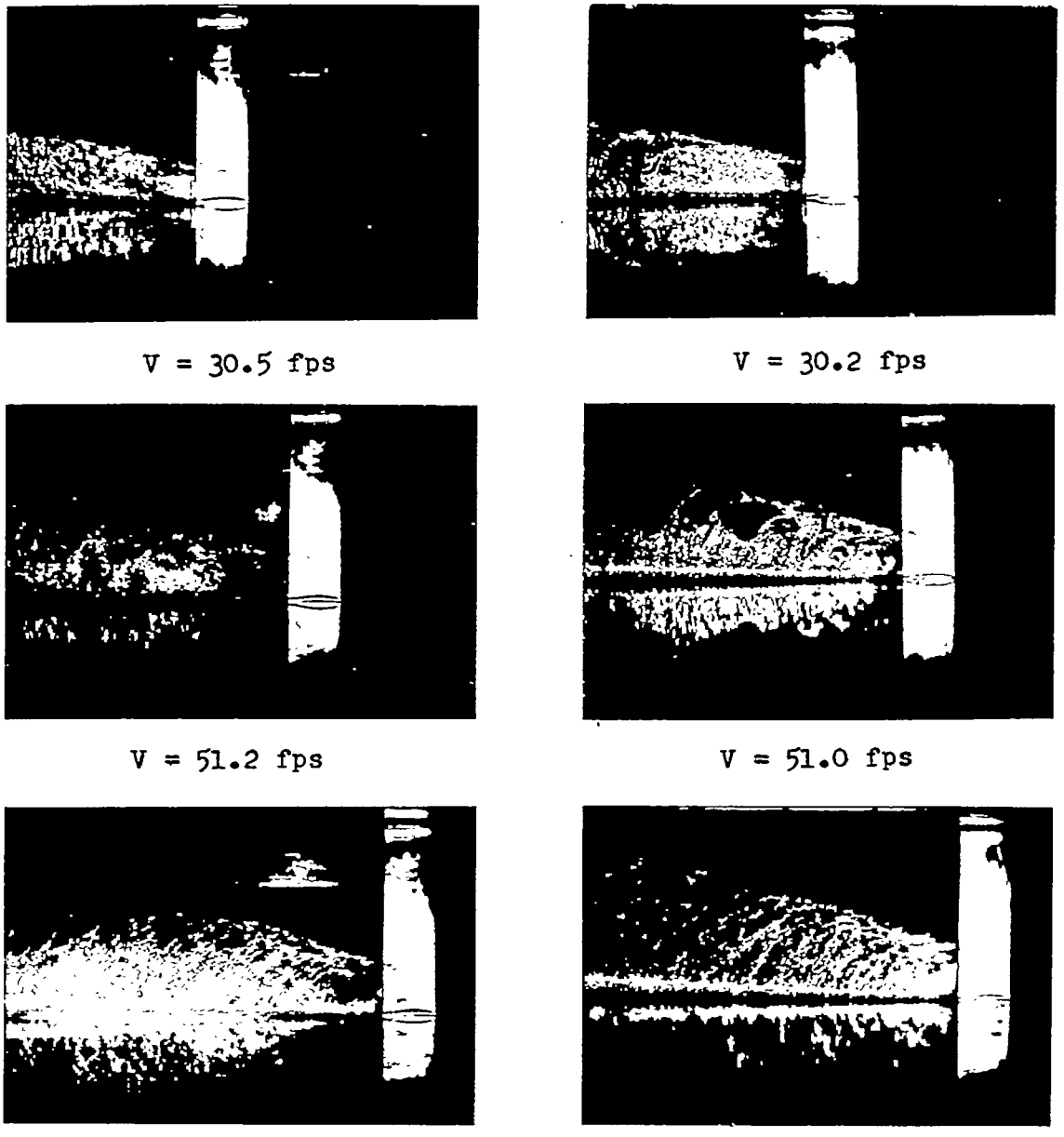

(a) 4-inch depth. (b) 24-inch depth.

Figure 8.- Photographs of strut spray. NACA 66_1-012 airfoil section with 4-inch chord; angle of rake, 0°.

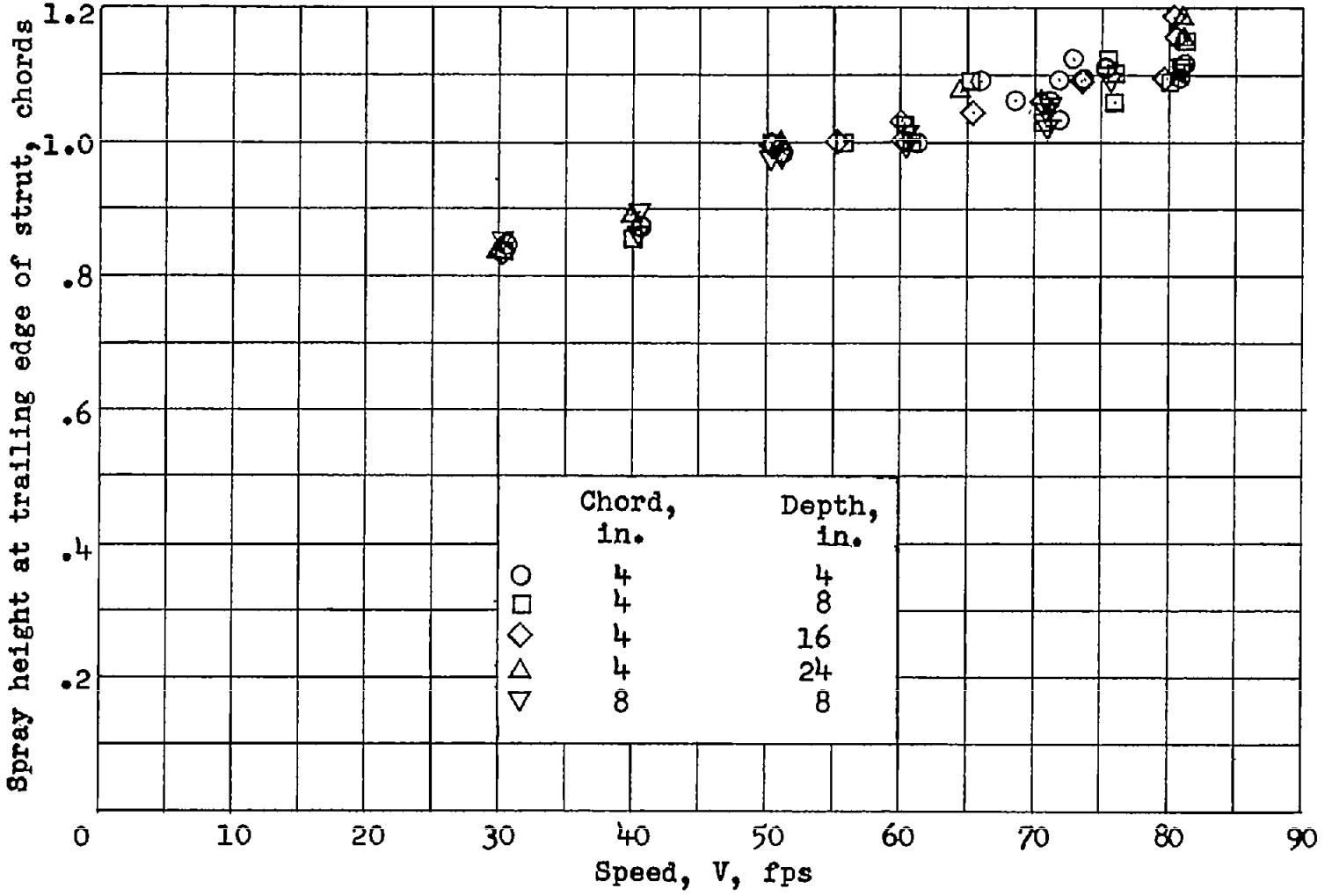

Figure 9.- Spray height at trailing edge of strut. NACA 66_1-012 airfoil section; angle of rake, 0°.

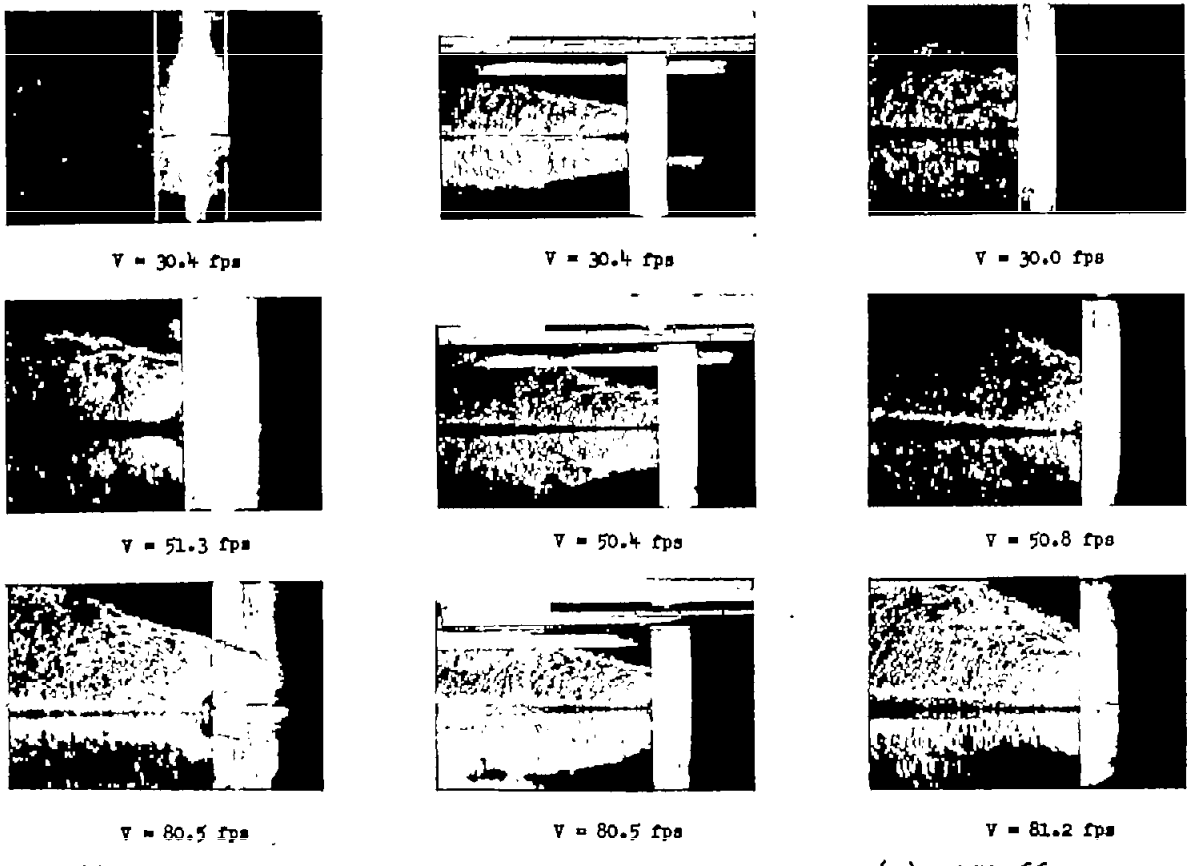

(a) NACA 66_1-012 airfoil section with 8-inch chord.

(b) NACA 66_1-012 airfoil section with 4-inch chord.

(c) NACA 66_4-021 airfoil section with 4-inch chord.

L-81267

Figure 10.- Photographs showing effect of strut size and thickness ratio on spray. Angle of rake, 0°.

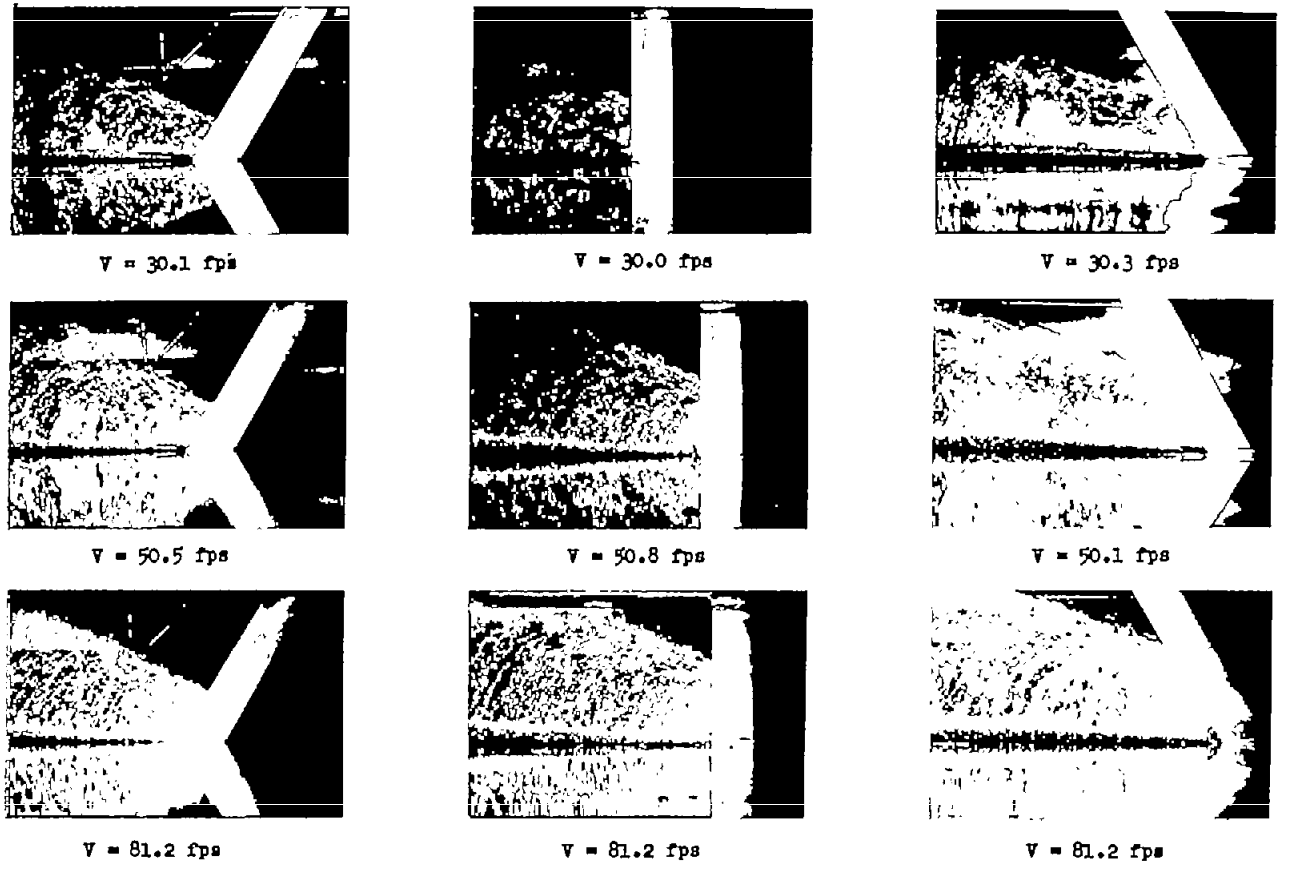

(a) Angle of rake, -30°. (b) Angle of rake, 0°. (c) Angle of rake, 30°.

L-81268

Figure 11.- Photographs showing effect of angle of rake on spray height. NACA 66_4-021 airfoil section; 4-inch chord.

V = 40.5 fps

V = 40.8 fps

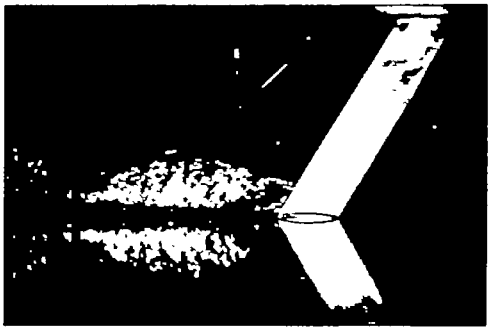

V = 50.6 fps

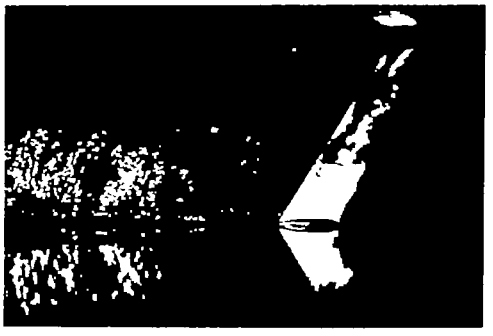

V = 50.5 fps

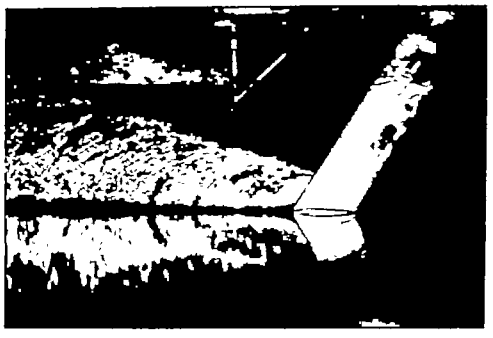

V = 82.0 fps

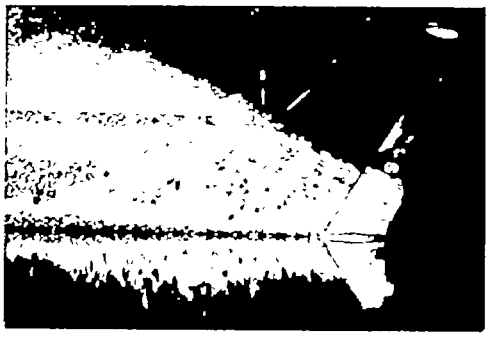

V = 81.2 fps

(a) NACA 66_1-012 airfoil section.

(b) NACA 66_4-021 airfoil section.

L-81269

Figure 12.- Photographs showing effect of thickness ratio on spray height. 4-inch chord; angle of rake, -30°.

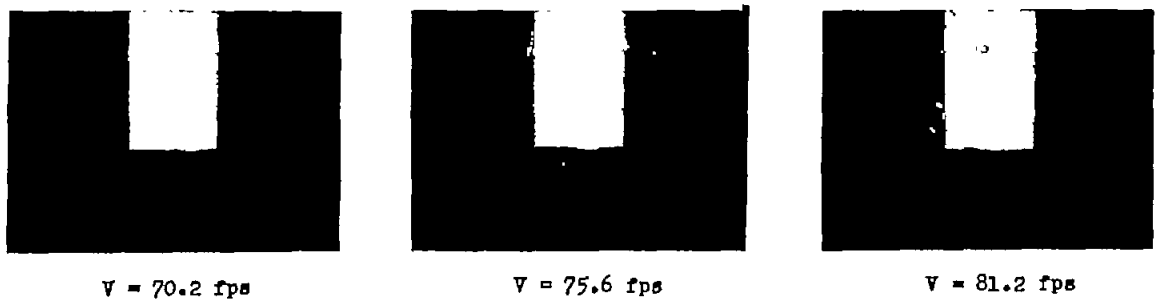

V = 70.2 fps V = 75.6 fps V = 81.2 fps

(a) 4-inch depth.

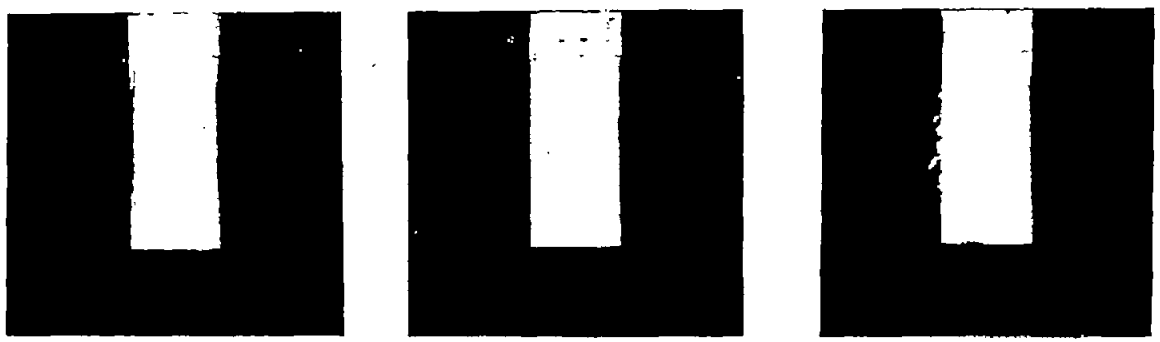

V = 66.0 fps V = 67.4 fps V = 75.8 fps

L-81270

(b) 8-inch depth.

Figure 13.- Effect of speed on cavitation. NACA 66_4-021 airfoil section; 4-inch chord; angle of rake, 0°.

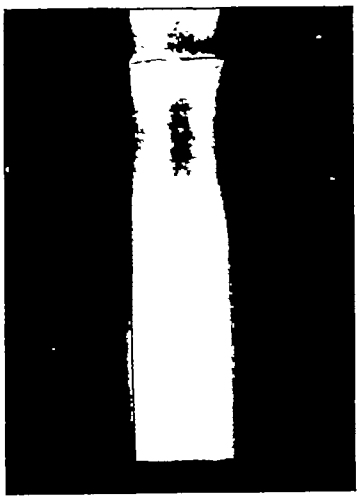

V = 63.1 fps

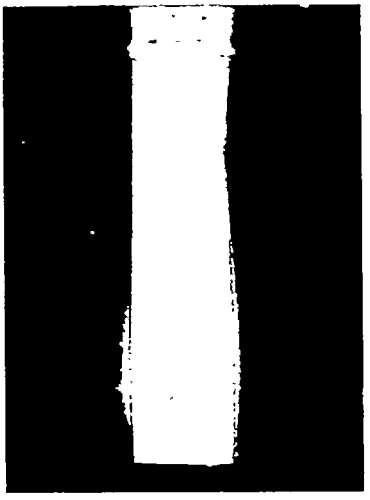

V = 67.0 fps

(c) 16-inch depth.

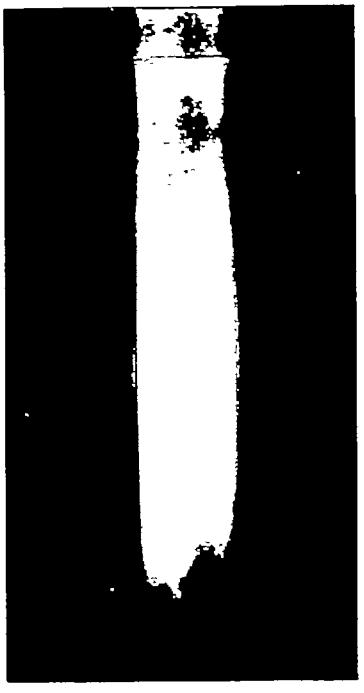

V = 65.3 fps

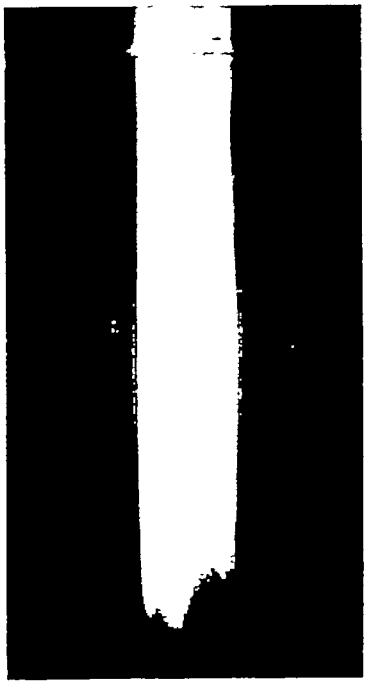

V = 67.2 fps

L-81271

(d) 24-inch depth.

Figure 13.- Concluded.

NACA-Langley - 12-18-53 - 1000